Eur. Phys. J. B **37**, 321–327 (2004)
DOI: 10.1140/epjb/e2004-00062-8

THE EUROPEAN PHYSICAL JOURNAL B

Structural studies of $La_{1-x}Sr_xMnO_{3+\delta}$ (x = 0.1–1.0)

R. Bindu[a]

Inter University Consortium for DAE facilities, University Campus, Khandwa Road, Indore-452 017, India

Received 18 July 2003 / Received in final form 17 November 2003
Published online 2 April 2004 –

Abstract. We report here for the first time (particularly for $x \geq 0.5$) a systematic structural study using Rietveld Profile Refinement of powder X-ray diffraction data on the series of polycrystalline compounds $La_{1-x}Sr_xMnO_{3+\delta}$ ($0.1 \leq x \leq 1.0$). The iodometric redox titration results show that the compounds $0.1 \leq x \leq 0.4$ and the end compound are oxygen excess and deficient respectively and the compounds in the compositional range $0.5 \leq x \leq 0.9$ are oxygen stoichiometric within the experimental error. It is found that the structure remains hexagonal until $x = 0.4$ composition. On further doping, at $x = 0.5$ composition, a structural transition to orthorhombic phase is observed. Around this composition, very small variations in the Mn-O(2)-Mn and average Mn-Mn bond distances are observed. For above $x = 0.5$, until $x = 0.8$ composition, the structure remains orthorhombic with reduced orthorhombic distortion. For the next compound, $x = 0.9$, a mixed hexagonal and orthorhombic phase is observed where the hexagonal phase is 6 layered with stacking sequence of ABCACB type and the orthorhombic phase is more distorted than that of $x = 0.8$ composition. The end compound is a four layered hexagonal structure with stacking sequence ABAC type which is more distorted than ABCACB type. As one goes down the series, a decrease in the volume per formula unit and average Mn-O bond distance are observed except at $x = 0.9$ composition. The observed structural transitions from hexagonal to orthorhombic to layered hexagonal phase can be explained under the electrostatic limit.

PACS. 61.1.Nz X-ray diffraction – 75.47.Lx Manganites

1 Introduction

There is a considerable research activity [1–4] in the field of rare earth transition metal oxides. These compounds show unusual electronic and magnetic properties because of, firstly, the important role played by the electron-electron and electron-lattice interactions. The electron correlation effects are mainly due to the narrow electronic bands in the oxides of the *d*-block transition metal elements. Such bands are formed by reduced hybridization of the *d* orbital of transition metal ion and the *p* orbital of oxygen ion. The band width is typically of the order of 1 to 2 eV whereas it is found to be 5 to 15 eV in most of metals. Secondly, the oxygen stoichiometry in these materials is usually not perfect. These oxides with oxygen holes, i.e. with p^5 configuration instead of p^6, contain highly correlated valence electrons leading to polaronic and bipolaronic effects. Thirdly, some of the transition metal oxides show layered structures with transition metal-oxygen planes separated by rare earth ion and oxygen ions. These structures in a limiting sense go over to perovskites of the type ABO_3. Among perovskites, cobaltates show interesting high spin-low spin transition [5], while manganites show exotic phenomena like colossal magneto resistance, phase separation, charge ordering, magnetic ordering, metal insulator transition, pressure induced phase transition etc. Charge ordering has also been observed in strontium doped ferrites [6] like $La_{1/3}Sr_{2/3}FeO_3$. In these compounds electron correlations play very important role. Electron lattice interaction through the Jahn-Teller effect also affects the magnetic and transport properties. These compounds also exhibit ionic size effect depending on the applied chemical pressure, i.e. whether the ion is substituted in the A or B site. This would alter the bond distance and hence the band width (or electron hopping interaction). The doping level and the bandwidth control the kinetic energy of the conduction electrons, which governs the metal insulator transition and also the competing magnetic interaction.

$La_{1-x}Sr_xMnO_3$ is a very important material showing many of the exciting properties mentioned above. This is a well known double exchange system with Mn ion in 3+ and 4+ states. The relative percentage of the Mn^{3+} and Mn^{4+} is decided by strontium doping and oxygen vacancies. The end-compound $LaMnO_3$ shows strong Jahn-Teller effect resulting in further splitting of t_{2g} and e_g levels. This effect is expected to persist, though reduced, with doping.

[a] e-mail: bindu@iucindore.ernet.in

In these compounds considerable work on structural, magnetic and transport properties have been carried out on single crystals for the composition $x < 0.5$. The main interest in studying these compounds below 50% strontium doping is due to the emergence of colossal magneto resistance for $x = 0.3$ composition. In the case of single crystals around the composition $x = 0.8$, possibility of charge ordering has been predicted due to the sharp increase in resistivity at Néel temperature, T_N [7].

Recently Hemberger et al. [7] have reported the phase diagram (structural, magnetic and electrical properties) for a single crystal phase of $La_{1-x}Sr_xMnO_3$. At room temperature for the parent compound, $LaMnO_3$, different structures such as cubic, orthorhombic, monoclinic have been reported for stoichiometric and nonstoichiometric compounds [2,7,9,12]. For $x = 0.1$ compound, depending on the method of preparation, different authors [2,7,12,13] have reported orthorhombic and rhombohedral structures. In the range $0.2 \leq x \leq 0.5$, rhombohedral structure has been mostly reported [2,7,12,13]. However, a cubic structure for the compositions $x = 0.4$ and 0.5 has also been reported by Mahendiran et al. [12]. Above the half doped region. i.e. $x = 0.55$–0.85, Hemberger et al. [7] have reported tetragonal structure. For $x = 0.9$, hexagonal structure has been reported [15]. For the end-member, $SrMnO_3$,workers [7,8,18] have reported hexagonal, orthorhombic and cubic structures depending on the oxygen stoichiometry and the final sintering temperature. These compounds are very sensitive to the internal pressure which changes both the Mn-O bond distances and Mn-O-Mn bond angles affecting the hopping interaction and/or band width and hence the transport and the magnetic properties. These interesting behaviours prompted us to undertake a systematic structural study on entire series of $La_{1-x}Sr_xMnO_{3+\delta}$, $0.1 \leq x \leq 1.0$ using X-ray diffraction.

From iodometric redox titration we found that compounds $x \leq 0.4$ and $x = 1.0$ are oxygen nonstoichiometric and the compounds $0.5 \leq x \leq 0.9$ are nearly stoichiometric within the experimental error. The best fit obtained from the Rietveld profile refinement of powder X-ray diffraction patterns for $x = 0.5$ composition revealed an orthorhombic phase and a mixed hexagonal and orthorhombic phase for $x = 0.9$ composition. To the best of our knowledge this has been observed for the first time. With the increase in the percentage of strontium, the structure remains hexagonal until $x = 0.4$ and on further doping till $x = 0.8$, the structure is orthorhombic. The next compound shows hexagonal phase (6L, L=Layer) mixed with orthorhombic structure and the end-compound is hexagonal (4L). To the best of our knowledge this is the first report on a thorough structural analysis for this series of polycrystalline compounds, which may help in understanding the nature of transport and magnetic properties.

2 Experimental

Powdered samples of $La_{1-x}Sr_xMnO_{3+\delta}$ ($x = 0.1$–1.0 in steps of 0.1) were prepared by solid state reaction of

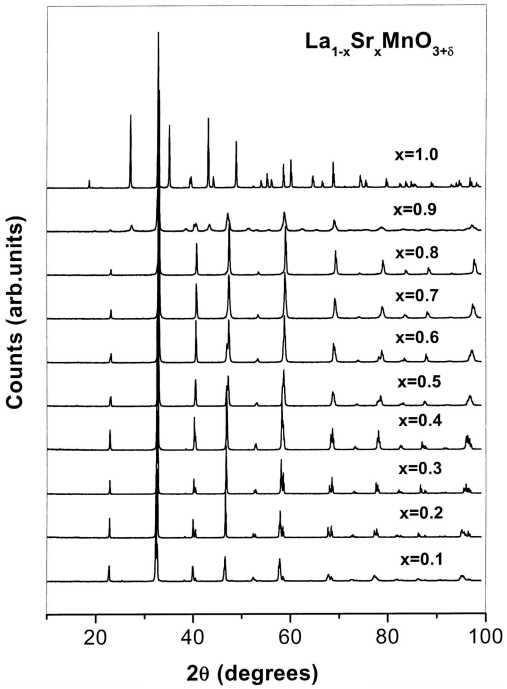

Fig. 1. The observed X-ray diffraction patterns for $La_{1-x}Sr_xMnO_{3+\delta}$ ($0.1 \leq x \leq 1.0$).

La_2O_3 (Leico 99.99%), $SrCO_3$ (Cerac 99.999%), MnO (Cerac 99.9%) with repeated grinding and calcinations at 1000 °C. The starting material used for $x = 0.8$, 0.9, 1.0 compounds were La_2O_3, $SrCO_3$, MnO_2(Cerac 99.9%). Final sintering for all the samples was done at 1400 °C for 2 days to have better crystalline quality. All the samples were studied by X-ray powder diffraction technique at room temperature. The X-ray powder diffraction patterns were recorded with monochromatised Cu-K_α radiation in the 2θ range of 10°–100° using Rigaku powder X-ray diffractometer. The rotating anode X-ray generator was operated at 50 KV and 120 mA. The monochromator used was graphite (002) and the widths of the divergent slit, scattering slit and the receiving slit were 0.5°, 0.5°, 0.15 mm respectively. The data were collected with a step size of 0.02° with a scanning rate of 2° per minute. The X-ray diffraction patterns were fitted using Rietveld X-ray profile refinement technique [10]. Iodometric redox titration was carried out using sodium thiosulphate and potassium iodide to estimate the percentage of Mn^{4+} ions.

3 Results and discussion

The iodometric titration results showed that for $x = 0.1$ compound, the percentage of Mn^{4+} ions is 18.3(3). For the range $0.2 \leq x \leq 0.4$, the percentage deviation of Mn^{4+} ions from their stoichiometric value was about 5–36% in excess and for $0.5 \leq x \leq 0.9$ it is within 5%. Hence the compounds in the range $0.5 \leq x \leq 0.9$ can be considered as stoichiometric. The end compound is oxygen deficient. The percentage of Mn^{4+} ions and the oxygen nonstoichiometry parameter δ are listed in Table 1.

The X-ray diffraction patterns for the whole series of the compounds are shown in Figure 1. Table 1 also gives

Table 1. Lattice parameters of $La_{1-x}Sr_xMnO_{3+\delta}$ ($0.1 \leq x \leq 1.0$) at room temperature obtained from Rietveld fitting and the percentage of Mn^{4+} ions and the oxygen nonstoichiometry parameter δ estimated from iodometric redox titration.

Sample x	Space group	Lattice parameters (Å)	Mn^{4+} (%)	δ	R_p (%)	R_{wp} (%)	R_e (%)	$S = (R_{wp}/R_e)$
0.1	R-3CH (94 wt%)	$a = 5.5325(4)$ $c = 13.3511(1)$	18.3(3)	0.041(1)	16.14	21.5	13.56	1.58
	Pm3m (6wt)%	$a = 3.9040(1)$						
0.2	R-3CH	$a = 5.5286(2)$ $c = 13.3672(2)$	27.1(6)	0.036(3)	14.87	20.6	14.15	1.45
0.3	R-3CH	$a = 5.5079(2)$ $c = 13.3569(2)$	34.6(1)	0.0231(1)	18.42	23.83	14.52	1.64
0.4	R-3CH	$a = 5.4839(2)$ $c = 13.3454(3)$	43.2(1)	0.0162(5)	11.14	15.37	10.52	1.46
0.5	Pbnm	$a = 5.4444(5)$ $b = 5.4449(5)$ $c = 7.7518(1)$	52.3(3)	0.012(1)	12.1	16.37	11.2	1.46
0.6	Pbnm	$a = 5.4257(2)$ $b = 5.4295(2)$ $c = 7.7342(2)$	62.2(9)	0.011(1)	11.84	15.71	10.7	1.47
0.7	Pbnm	$a = 5.4201(1)$ $b = 5.4172(1)$ $c = 7.6926(3)$	72.7(2)	0.013(1)	11.03	15.02	9.99	1.5
0.8	Pbnm	$a = 5.4083(3)$ $b = 5.4078(1)$ $c = 7.6586(3)$	83(1)	0.017(6)	13.11	18.51	10.95	1.69
0.9	P63/mmc (68 wt%)	$a = 5.4282(2)$ $c = 13.4278(3)$	89.0(6)	−0.005(1)	17.54	22.12	10.56	2.09
	Pbnm (32 wt%)	$a = 5.3930(7)$ $b = 5.4238(3)$ $c = 7.6934(1)$						
1.0	P63/mmc	$a = 5.4462(1)$ $c = 9.0755(1)$	93.2(8)	−0.034(4)	11.45	15.28	10.08	1.51

the lattice constants and space groups of these compounds ($x = 0.1$–1.0 in steps of 0.1) obtained from the Rietveld profile refinement software. The refinement of one of these compounds is shown in Figure 2 for illustration. Typically, our goodness of fit given by the parameter S (shown in the last column of Tab. 1) – the ratio of weighted pattern and expected pattern (R_{wp}/R_e) – is around 1.5. For the end-member of the series (in Tab. 1 it is for $x = 0.9$), however, this parameter is slightly larger – 2.1, although the fit is still quite good and comparable to the published literature [15]. The data of Table 1 is then used to calculate bond distances and the bond angles using Powder Cell software [11], which are given in Table 2.

In $LaMnO_3$, Mn is in 3+ state with 4 valence electrons in the $3d$ orbital. Crystal field splits d orbitals into three fold $t_{2g}(d_{xy}, d_{yz}, d_{zx})$ and two fold e_g $(d_{x^2-y^2}, d_{3z^2-r^2})$ levels. The t_{2g} orbitals are not directed towards the oxygen $2p$ orbitals, which are along coordinate axes and hence, are less strongly hybridized with them. The e_g orbitals point directly towards the oxygen $2p$ orbitals and interact strongly with them. One can thus consider the three electrons in t_{2g} orbitals as localised and the lone electron in e_g orbitals as itinerant in character. It is well known [1]

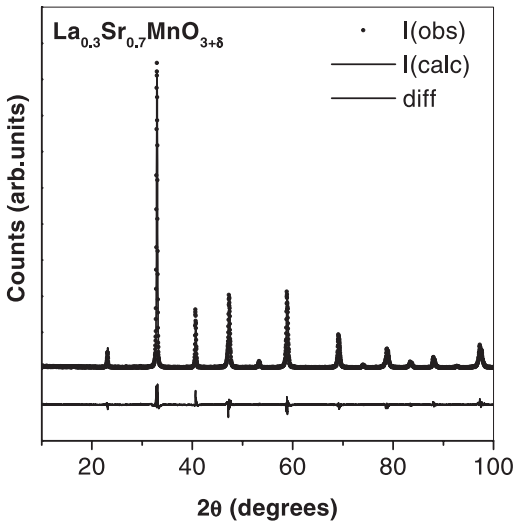

Fig. 2. The X-ray diffraction pattern of $La_{0.3}Sr_{0.7}MnO_{3+\delta}$. The solid circles and the solid line indicate the experimental (I_{obs}) and the Rietveld refined (I_{calc}) X-ray diffraction profile respectively. The lower part of the figure shows the difference plot (I_{obs}–I_{calc}).

Table 2. Bond distances (Å), bond angles (in degrees) of $La_{1-x}Sr_xMnO_{3+\delta}(0.1 \leq x \leq 1.0)$.

$La_{1-x}Sr_xMnO_{3+\delta}$	Mn-O(1) (Å)	Mn-O(2) (Å)	Mn-O(2) (Å)	Mn-O(2)-Mn (in degrees)	Mn-O(1)-Mn (in degrees)	Average (Å)
$La_{0.9}Sr_{0.1}MnO_{3+\delta}$	1.9844(1)			157.56(6)		3.8929(4)
$La_{0.8}Sr_{0.2}MnO_{3+\delta}$	1.9638(2)			164.7(1)		3.8925(2)
$La_{0.7}Sr_{0.3}MnO_{3+\delta}$	1.9535(1)			166.9(1)		3.8818(2)
$La_{0.6}Sr_{0.4}MnO_{3+\delta}$	1.9422(9)			169.9(7)		3.8693(3)
$La_{0.5}Sr_{0.5}MnO_{3+\delta}$	1.958(2) × 2	2.06(2) × 2	1.80(3) × 2	170.2(8)	163.5(8)	3.8629(4)
$La_{0.4}Sr_{0.6}MnO_{3+\delta}$	1.954(2) × 2	2.02(1) × 2	1.84(2) × 2	168.7(3)	163.5(5)	3.8525(2)
$La_{0.3}Sr_{0.7}MnO_{3+\delta}$	1.9272(8) × 2	2.02(1) × 2	1.818(7) × 2	172(2)	172.6(6)	3.8389(2)
$La_{0.2}Sr_{0.8}MnO_{3+\delta}$	1.925(3) × 2	2.027(2) × 2	1.797(2) × 2	179.3(8)	168(1)	3.8267(3)
$La_{0.1}Sr_{0.9}MnO_{3+\delta}$	2.008(2)[a] × 3	1.88(1)[b] × 3	1.883(8)[c] × 6	173(2)[d]	79(2)[e]	2.5555(6)
	1.950(2) × 2	**2.211(5) × 2**	**1.619(5) × 2**	**174.2(2)**	**161.1(7)**	**3.8267(4)**
$SrMnO_{3+\delta}$	1.8736(1) × 3	1.889(9) × 3		180	82.9(4)	2.5000(7)

a = Mn(2)-O(1); b =Mn(2)-O(2); c = Mn(1)-O(2); d = Mn(1)-O(2)-Mn(2); e = Mn(2)-O(1)-Mn(2). The atomic positions for Orthorhombic structure (Pbnm): La/Sr: $4c(x, y, 1/4)$, Mn: $4b(0, 1/2, 0)$, O(1): $4c(x, y, 1/4)$, O(2): $8d(x, y, z)$; for Hexagonal structure(R3-CH): La/Sr: $6a(0, 0, 1/4)$, Mn: $6b(0, 0, 0)$, O: $18e(x, 0, 1/4)$; for Hexagonal (P63/mmc)(4L): La/Sr(1): $2b(0, 0, 1/4)$, La/Sr(2): $4f(1/3, 2/3, z)$, Mn(1): $2a(0, 0, 0)$, Mn(2): $4f(1/3, 2/3, z)$, O(1): $6h(x, -x, 1/4)$, O(2): $12k(x, -x, z)$. Hexagonal(P63/mmc)(6L): Sr(1): $4e(00z)$, Sr(2): $2c(1/3, 2/3, 1/4)$, Mn: $4f(1/3, 2/3, z)$, O(1): $6g(1/2, 0, 0)$, O(2): $6h(-x, x, 3/4)$. The values of the bond distances and bond angles given in bold corresponds to the orthorhombic phase of $x = 0.9$ composition.

Table 3. Volume per formula unit and average Mn-O bond distances for $La_{1-x}Sr_xMnO_{3+\delta}$ $(0.1 \leq x \leq 1.0)$.

$La_{1-x}Sr_xMnO_{3+\delta}$	Structure	Volume (Å^3)	Volume/formula unit (Å^3)	Av. Bond distance (Å)	$c/\sqrt{2}a$
$La_{0.9}Sr_{0.1}MnO_{3+\delta}$	H + C	353.9(1) + 59.50(1)	58.98(10) + 59.50(1)	1.9844(4)	
$La_{0.8}Sr_{0.2}MnO_{3+\delta}$	H	353.84(6)	58.97(6)	1.9638(2)	
$La_{0.7}Sr_{0.3}MnO_{3+\delta}$	H	350.95(6)	58.49(6)	1.9535(1)	
$La_{0.6}Sr_{0.4}MnO_{3+\delta}$	H	347.57(7)	57.93(7)	1.9422(9)	
$La_{0.5}Sr_{0.5}MnO_{0+\delta}$	O	229.80(9)	57.45(9)	1.941(1)	1.006
$La_{0.4}Sr_{0.6}MnO_{3+\delta}$	O	227.84(4)	56.96(4)	1.9367(1)	1.008
$La_{0.3}Sr_{0.7}MnO_{3+\delta}$	O	225.87(4)	56.47(4)	1.922(2)	1.004
$La_{0.2}Sr_{0.8}MnO_{3+\delta}$	O	223.99(5)	55.99(5)	1.9160(8)	1.001
$La_{0.1}Sr_{0.9}MnO_{3+\delta}$	H′ + O	342.65(4) + 225.04(9)	57.11(4) + 56.26(9)	1.925(8) + 1.9269(1)	
$SrMnO_{3+\delta}$	H′	233.13(2)	58.28(2)	1.881(4)	

H = Hexagonal (R-3CH), O = Orthorhombic (Pbnm), H′ = Hexagonal (P63/mmc).

that $LaMnO_3$ has two types of distortions of the MnO_6 octahedra; one is the cooperative rotation of the MnO_6 octahedra about different axes giving orthorhombic structure with lattice parameters $a \approx b = \sqrt{2}a_c$, $c = 2a_c$ where a_c is the lattice parameter of cubic unit cell. The second type of distortion is the Jahn-Teller distortion arising from electron-phonon coupling and an alternative elongation of the MnO_6 octahedra along the x and y axes, which are in the [110] and [1-1 0] directions of the orthorhombic unit cell. It leads to different Mn-O bond lengths for the three lengths involved in the MnO_6 octahedra due to different bond strengths corresponding to the split e_g orbitals involved in bonding.

When La is replaced partially by divalent Sr ions, some Mn ions go to 4+ state from Mn^{3+} state to conserve charge. It is well known that Mn^{4+} is not Jahn-Teller active, and thus one expects the MnO_6 octahedra to be less distorted. We find that for 10% Sr doping i.e. $x = 0.1$ composition (18.3(3)% of Mn^{4+}), the XRD pattern can be fitted to hexagonal phase (R-3CH) mixed with 6 wt% of cubic phase (Pm3m). The conditions, limiting possible reflections of X-ray peaks for hexagonal structure of space group R3-CH are $l = 2n$ for $hkil$. For further Sr doping till $x = 0.4$, the sample remains in a pure hexagonal (R-3CH) phase accompanied by reduction in volume per formula unit and the bond distances as shown in Table 3. The MnO_6 octahedra in these structures have only one Mn-O bond length and show less distortion in the Mn-O-Mn bond angles (given in Tab. 2). The hexagonal unit cell contains 6 formula units.

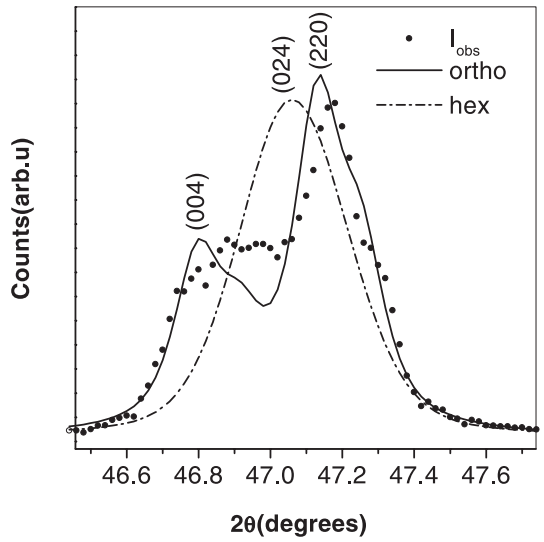

Fig. 3. Rietveld fitting of XRD pattern in the 2θ range $46.45°$–$47.73°$ for $La_{0.5}Sr_{0.5}MnO_{3+\delta}$. The solid circle, solid line and solid dash dot indicate the experimental XRD pattern, orthorhombic fit and hexagonal fit respectively. It is clearly seen that the pattern is better fitted to 2 peaks given by orthorhombic structure rather than a single peak arising from hexagonal structure.

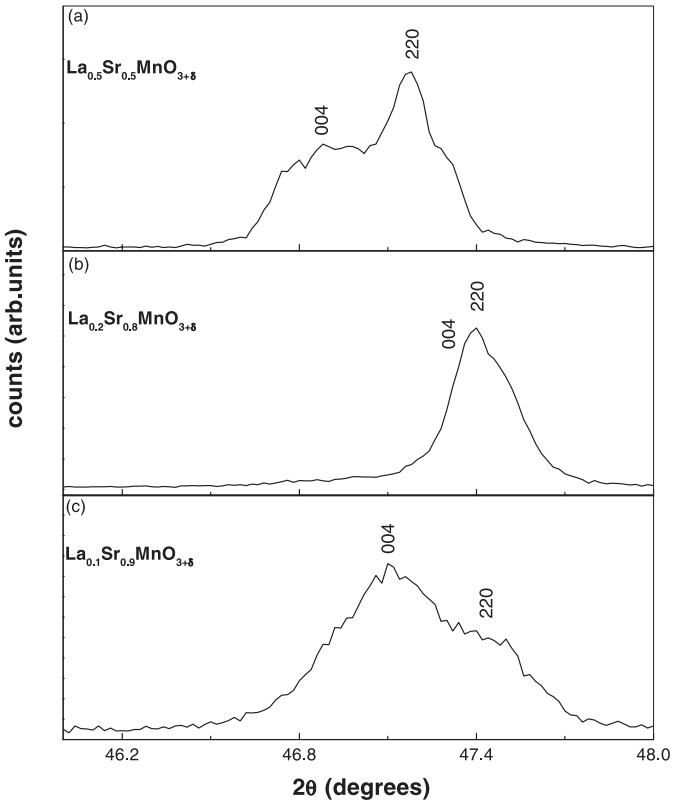

Fig. 4. (004) and (220) diffraction peaks for $La_{1-x}Sr_xMnO_{3+\delta}$ (a) $x = 0.5$ and (b) $x = 0.8$ (c) $x = 0.9$. The separation in the peaks decreases with increased strontium content and merge at $x = 0.8$ composition. It further splits at $x = 0.9$ composition. For the $x = 0.9$ composition in the orthorhombic phase, the (004) peak intensity is greater than (220) peak intensity indicating an increase in the lattice parameter along the c-axis. The decrease in the separation of the peaks indicates the decrease of the orthorhombic distortion and at $x = 0.9$, the orthorhombic distortion further increases.

For $x = 0.5$, cubic as well as rhombohedral structures have been reported in the literature [7,9,12]. In our case, there is 52.3(3)% of Mn^{4+} ions which is close to stoichiometry, the data could not be fitted to cubic structure as the split in the diffraction peaks at 2θ values of 32.5°, 32.7° and also peaks at higher angles cannot be accounted by cubic fitting. Also, the rhombohedral structure after conversion to hexagonal shows only one peak at (024) position. The fit to the experimental data assuming cubic or rhombohedral structures in this region is rather poor. However, orthorhombic structure can be better fitted as it gives doublet at these positions. The fit is shown in Figure 3. The conditions, limiting the possible reflections for orthorhombic phase belonging to Pnma space group are $k+l = 2n$ for $0kl$, $h = 2n$ for $hk0$, $h = 2n$ for $h00$, $k = 2n$ for $0k0$, $l = 2n$ for $00l$. Thus, we find that the complete diffraction pattern is better fitted to orthorhombic (Pbnm) structure than the rhombohedral structure (R-3CH). The structure remains orthorhombic until $x = 0.8$, although with a small reduction in lattice constants as Sr content increases. In this range ($0.5 \leq x \leq 0.8$), with the increase in the strontium percentage, the $c/\sqrt{2}a$ ratio also approaches 1 indicating an increased symmetry (Tab. 3). This is consistent with the observed decrease in the splitting of the (004) and (220) peaks with increased strontium doping. Figure 4 shows the (004) and (220) peaks for the two end-compositions of orthorhombic structure $x = 0.5$ and $x = 0.8$. Similar behaviour was also seen by Hemberger et al. [7]. Around $x = 0.5$ composition, a very small variation in the Mn-O(2)-Mn bond angle and average Mn-Mn bond distances are observed as one goes down the series, shown in Table 2. Since there is no significant change in the average Mn-Mn bond distances around $x = 0.5$ composition, the only way (under the electrostatic limit) for the system to attain minimum energy configuration is by the rotation of the MnO_6 octahedra and hence orthorhombic structure. The Mn-O(2)-Mn bond angle further increases on strontium doping in the range $0.5 \leq x \leq 0.8$. As the Mn-O(2)-Mn bond angle increases, the Mn-O(1) bond distance decreases in such a way that there is a decrease in the average Mn-Mn bond distance. The reduction in the orthorhombic distortion above $x = 0.5$ composition until $x = 0.8$ composition can be explained in the electrostatic limit as follows. For a stoichiometric compound, on doping x percentage of Sr^{2+} at the La^{3+} site, x percentage of Mn^{3+} is converted to Mn^{4+}; these Mn^{4+} ions may be considered to be distributed uniformly in the whole crystal lattice. In the case of the perovskite structure, all the MnO_6 octahedra are corner linked with the neighbouring MnO_6 octahedra. The Coulombic repulsion between different manganese ions are in the following order Mn^{3+}-Mn^{3+} $< Mn^{3+}$-$Mn^{4+} < Mn^{4+}$-Mn^{4+} ions. Since the Mn^{4+}-O^{2-} ions experience more Coulombic attraction than Mn^{3+}-O^{2-}, we expect the Mn^{4+}-O^{2-} bond distances

to be reduced compared to Mn^{3+}-O^{2-} bond distances. Therefore, as the Mn^{4+} content increases on strontium doping, a reduction in the average Mn-O bond distances is observed. Following the reduction in the average Mn-O bond distance, the volume of the MnO_6 octahedra reduces which would further lead to a decrease in the lattice parameters in such a way that the $c/\sqrt{2}a$ ratio also decreases and approaches unity and hence reduced orthorhombic distortion.

For the composition $x = 0.9$, hexagonal structure has been reported [15]. The crystal structure is similar to that of $BaTiO_3$ [16]. In our case, the $x = 0.9$ compound is close to stoichiometry with 89.0(6)% of Mn^{4+} ions and we observe hexagonal structure (Pbnm) mixed with 32 wt% of orthorhombic phase (P63/mmc). The orthorhombic structure was chosen as the second phase because the peaks observed at 2θ values 47.11° and 47.39° are better fitted to orthorhombic structure which corresponds to the reflection planes, (004) and (220); the hexagonal structure gives only one peak at 47.02° corresponding to the (024) reflection plane. The conditions, limiting possible reflections of X-ray peaks for hexagonal structure which corresponds to the space group P63/mmc, are $l = 2n$ for $hkil$, if $h - k = 3n$, then $l = 2n$ for $hkil$. The hexagonal phase contains 6 formula units. This compound shows a six closed packed layer with SrO_3 layers stacked in ABCACB sequence where A is the cubic layer, B and C are the hexagonal layers. In this structure two-thirds of the MnO_6 octahedra are face-shared, forming Mn_2O_9 coordination group, and, one-third of the MnO_6 octahedra are corner-shared to the Mn_2O_9 coordination group. With the increase in the strontium doping it is observed that the average metal-metal bond distance decreases, indicating the increase in the Coulombic interaction of the metal-metal ion. Because of the smaller size of the Mn^{4+} ion, the surrounding oxygen ions arrange themselves to screen the Coulombic repulsion of the metal-metal ion. Due to this reason MnO_6 octahedra is distorted for $x = 0.9$ composition in the hexagonal phase. This distortion becomes more remarkable when the effective size of the octahedral site becomes smaller. This leads to the observation of layered structure for $x = 0.9$ composition. The orthorhombic phase contains 4 formula units. For $x = 0.8$ composition, the (004) and the (220) peaks are merged; these split in the case of $x = 0.9$ with (004) peak intensity larger than (220) peak intensity indicating an elongation of the lattice parameter along the c axis for $x = 0.9$ composition. In the case of $x = 0.5$ composition, the reverse is observed. The split in the (004) and (220) peaks indicate the reoccurrence of orthorhombic distortion shown in Figure 4. As we go from $x = 0.8$ to $x = 0.9$ composition, the following changes are observed (a) increase in the volume per formula unit and average Mn-O bond distances (b) reduction in the Mn-O(2)-Mn bond angles, (c) the average Mn-Mn bond distances remains unchanged. Since no variation in the average Mn-Mn bond distances are observed and also the Mn^{4+}ionic radii are small compared to the ionic radii of Mn^{3+}, for the orthorhombic structure to remain stable, the oxygen ions rearrange themselves leading to distortion. Hence, for $x = 0.9$ composition, the orthorhombic distortion is more as compared to $x = 0.8$ composition. The end-compound is hexagonal (P63/mmc) and oxygen deficient with 93.2(8)% of Mn^{4+} ions. The conditions, limiting possible reflections for hexagonal structure of space group P63/mmc are $l = 2n$ for $hkil$; if $h - k = 3n$, then $l = 2n$ for $hkil$; if $h - k = 3n$, then $l = 2n$ for $hkil$. The hexagonal unit cell contains 4 formula units. The SrO_3 layers are stacked along the hexagonal c axis with ABAC sequence. Vacancy created in the cubic layer (A) leads to the face-sharing of the trigonal bipyramid with the MnO_6 octahedron and the vacancy created in the hexagonal layer (B or C) leads to the edge-sharing of the trigonal bipyramids which are linked to the face-shared octahedra by corner sharing. For this compound, the average Mn-Mn bond distance is about 2.5 Å with a strong Coulombic repulsion between the metal ions. Since the Coulombic repulsion experienced is much stronger, the distortion in the MnO_6 octahedra is very large compared to that of the hexagonal phase of the $x = 0.9$ composition leading to a reduction in the lattice parameter along the c-axis and hence the stacking sequence of ABAC type. Thus with the increase in the strontium doping it is natural to expect a phase transformation of ABC type – ABCACB type – ABAC type.

To summarize, it is observed that as the strontium level increases, the system goes from a perovskite type structure to a layered structure. In the process of change in the crystal structure we observe a decrease in the average Mn-Mn bond distance and also a slight decrease in the unit cell volume per formula unit i.e. from 58.98 $Å^3$ to 58.28 $Å^3$, except at $x = 0.9$ composition. The increase in the volume per formula unit for $x = 0.9$ composition may be due to the increase in the distortion of the MnO_6 octahedra leading to structural transition to an admixture of perovskite and a layered type structures. It is to be noted that there is a changeover in the Mn-O(2)-Mn bond angle (basal plane) and also a very less significant change in the average Mn-Mn bond distance around the compositions where structural transition is seen.

4 Conclusion

We report systematic detailed structural studies on polycrystalline $La_{1-x}Sr_xMnO_{3+\delta}$. From iodometric redox titration we found that the compounds $x \leq 0.4$ and end compound are oxygen excess and deficient respectively and the compounds $0.5 \leq x \leq 0.9$ are oxygen stoichiometric within the experimental error. In this work we have shown that $La_{1-x}Sr_xMnO_{3+\delta}$ compounds crystallise in perovskite type and layered type structure.

As we go down the series we observe the following features: structural transition from hexagonal to orthorhombic to hexagonal (4L) + orthorhombic to hexagonal (6L).

(a) A decrease in volume per formula unit and decrease in average Mn-O bond distance except at $x = 0.9$ composition are observed.
(b) A structural transition to orthorhombic phase is observed around $x = 0.5$ composition and on further

increase in strontium doping, the structure remains orthorhombic until $x = 0.8$ composition with reduced orthorhombic distortion which is reflected in the $c/\sqrt{2}a$ ratio which approaches 1 and is consistent with a decrease in the splitting of the (004) and (220) peaks.

(c) The structural transitions can be explained under the electrostatic limit.

(d) For the $x = 0.9$ composition, we observe a hexagonal phase mixed with an orthorhombic phase where the hexagonal phase is a layered structure with ABCACB stacking sequence and the orthorhombic phase is more distorted.

(e) As the size of the octahedral site becomes smaller and smaller we observe a further distortion in the MnO_6 octahedra leading to a four layered structure. The end compound is oxygen deficient and is of hexagonal structure with stacking sequence ABAC.

Hence with the increase in the strontium doping, we observe a phase transformation of ABC type – ABCACB type – ABAC type. This study would be useful in understanding of the transport and magnetic properties where the structure plays a major role. We have also carried out near edge structure and EXAFS studies on the entire series of compounds and this will be reported elsewhere.

My special thanks to A.V. Pimpale for useful discussions and comments on the manuscript. I thank V.G. Sathe, N.P. Lalla, Ashna Bajpai and Ashwani Kumar for their invaluable help. I would also like to thank Manju for her initial help in iodometric titration. I am grateful to IUC-DAEF for the award of SRF.

References

1. Yoshinori Tokura, *Colossal Magnetoresistive Oxides* (Gordon and Breach, London, 2000)
2. J.M.D. Coey, M. Viret, S .Von Molnar, Adv. Phys. **48**, 167 (1999)
3. Y. Tokura, Y. Tomioka, J. Mag. Mag. Mater. **200**, 1 (1999)
4. C.N.R. Rao, Ann. Rev. Phys. Chem **40**, 291 (1989)
5. V.G. Sathe, A.V. Pimpale, V. Siruguri, S.K. Paranjpe, J. Phys: Condens. Matter **8**, 3889 (1996)
6. T. Ishikawa, S.K. Park, T. Katsufuji, T. Arima, Y. Tokura, Phys. Rev. B **58**, R13326 (1998)
7. J. Hemberger, A. Krimmel, T. Kurz, H.-A. Krug Von Nidda, Phys. Rev. B **66**, 094410 (2002)
8. J.F. Mitchell, D.N. Argyriou, C.D. Potter, D.G. Hinks, J.D. Jorgensen, S.D. Bader, Phys. Rev. B **54**, 6172 (1996)
9. A. Urushibara, Y. Moritomo, T. Arima, A. Asamitsu, G. Kido, Y. Tokura, Phys. Rev. B **51**, 14103 (1995)
10. R.A. Young, A. Sakthivel, J. Appl. Cryst. **21**, 416 (1988)
11. W. Kraus, G. Nolze, J. Appl. Cryst. **29**, 301 (1996)
12. R. Mahendiran, S.K. Tiwary, A.K. Ray Chaudhari, T.V. RamaKrishnan, Phys. Rev. B **53**, 3348 (1996)
13. Takanori Mori, Kazuko Inoue, Naoki Kamegashira, J. Alloys Comp. **308**, 87 (2000)
14. S.J. Hibble, S.P. Cooper, A.C. Hannon, I.D. Fawcett, M.Greenblatt, J. Phys: Condens. Matter **11**, 9221 (1999)
15. Takanori Mori, Naoki Kamegashira, J. Alloys Comp. **313**, L1 (2000)
16. R.D. Burbank, H.T. Evans, J. Acta Cryst. **1**, 330 (1948)
17. Yasuhiko Syono, S. Akimoto, J. Phys. Soc. Jpn **26**, 993 (1969)
18. T. Negas, R. Roth, J. Solid State Chem. **1**, 409 (1970)